

A Critical Study on Acylating and Covalent Reversible Fragment Inhibitors of SARS-CoV-2 Main Protease Targeting the S1 Site with Pyridine

Rebekka Wamser,^[a] Szymon Pach,^[a] Christoph Arkona,^[a] Morris Baumgardt,^[b] Umer Bin Abdul Aziz,^[a] Andreas C. Hocke,^[b] Gerhard Wolber,^[a] and Jörg Rademann^{*[a]}

SARS coronavirus main proteases (3CL proteases) have been validated as pharmacological targets for the treatment of coronavirus infections. Current inhibitors of SARS main protease, including the clinically admitted drug nirmatrelvir are peptidomimetics with the downsides of this class of drugs including limited oral bioavailability, cellular permeability, and rapid metabolic degradation. Here, we investigate covalent fragment inhibitors of SARS M^{Pro} as potential alternatives to peptidomimetic inhibitors in use today. Starting from inhibitors acylating the enzyme's active site, a set of reactive fragments was synthesized, and the inhibitory potency was correlated with the chemical stability of the inhibitors and the kinetic

stability of the covalent enzyme-inhibitor complex. We found that all tested acylating carboxylates, several of them published prominently, were hydrolyzed in assay buffer and the inhibitory acyl-enzyme complexes were rapidly degraded leading to the irreversible inactivation of these drugs. Acylating carbonates were found to be more stable than acylating carboxylates, however, were inactive in infected cells. Finally, reversibly covalent fragments were investigated as chemically stable SARS CoV-2 inhibitors. Best was a pyridine-aldehyde fragment with an IC₅₀ of 1.8 μM at a molecular weight of 211 g/mol, showing that pyridine fragments indeed are able to block the active site of SARS-CoV-2 main protease.

Introduction

The global outbreak of the coronavirus SARS-CoV-2, the seriousness of the disease COVID-19, the limited efficacy of vaccines, and the rapid formation of immune-escape mutations created an urgent need for antiviral drugs against this disease. The viral 3C-like protease (3CL^{Pro}), also called main protease (M^{Pro}), has been identified as pharmacological target for the treatment of the disease with small-molecule drugs.^[1] The catalytic site of the protease contains a catalytic dyad consisting of the negatively charged Cys145 and the protonated His41 residues.^[2] The cleavage of the peptide bonds is performed at glutamine in P1 through the nucleophilic attack of the Cys145.^[3] The main protease of the new coronavirus has structures similar to the previous main protease of SARS-CoV-1 with approximately 96% amino acid sequence identity.^[4] With 3C proteases (3C^{Pro}) from

picornaviruses such as rhinoviruses, coxsackieviruses, or other enteroviruses, 3CL proteases share the substrate specificity for glutamine in the P1 position and the catalytic mechanism.^[5,6] First inhibitors of SARS-CoV M^{Pro} were peptide mimetics carrying the glutamine side chain in P1 (Figure 1).^[7] Replacement of the native glutamine residue with pyrrolidine-2-one resulted in more potent inhibitors. This substitution originated from 3C protease inhibitors such as the milestone rupintrivir, which, nevertheless, failed in advanced clinical trials.^[8] Recently, the peptidomimetic nirmatrelvir showed broad-band antiviral activity against coronaviruses and was authorized for clinical use in the US and in the European Union against COVID-19 after reducing hospitalization or deaths in clinical trials significantly.^[9] Another well characterized inhibitor is the dipeptide GC376, not only being active against the main protease of SARS-CoV-2 but also against other 3CL proteases.^[10] All these peptidomimetic inhibitors targeting the S1 pocket with amide residues displayed high affinities to the target, however, the cellular permeability, the oral bioavailability, or the metabolic stability of such compounds were problematic. For example, nirmatrelvir needs to be used in an oral drug in combination with ritonavir, a potent inhibitor of cytochrome P450 3A4, to protect the γ-lactam (or pyrrolidin-2-one) residue from rapid oxidation.^[9a,11] For these reasons, the investigation of fragment-based protease inhibitors targeting the S1 site can be an attractive alternative to peptidomimetic inhibitors. In previous works, we and others have demonstrated that peptidomimetics containing glutamine residues or their lactam derivatives can be replaced successfully by druglike inhibitory fragments. Typically, these fragment inhibitors contained an aromatic amide such as benzamide or an amino-pyrazoline fragment for targeting the S1 pocket and a

[a] R. Wamser, Dr. S. Pach, Dr. C. Arkona, U. B. A. Aziz, Prof. Dr. G. Wolber, Prof. Dr. J. Rademann
Department of Biology, Chemistry and Pharmacy
Institute of Pharmacy, Freie Universität Berlin
Königin-Luise-Str.2 +4, 14195 Berlin (Germany)
E-mail: joerg.rademann@fu-berlin.de

[b] M. Baumgardt, Prof. Dr. A. C. Hocke
Department of Infectious Diseases, Respiratory Medicine and Critical Care
Charité – Universitätsmedizin Berlin, corporate member of Freie Universität
Berlin and Humboldt-Universität zu Berlin
Charitéplatz 1, 10117 Berlin (Germany)

Supporting information for this article is available on the WWW under <https://doi.org/10.1002/cmdc.202200635>

© 2023 The Authors. ChemMedChem published by Wiley-VCH GmbH. This is an open access article under the terms of the Creative Commons Attribution License, which permits use, distribution and reproduction in any medium, provided the original work is properly cited.

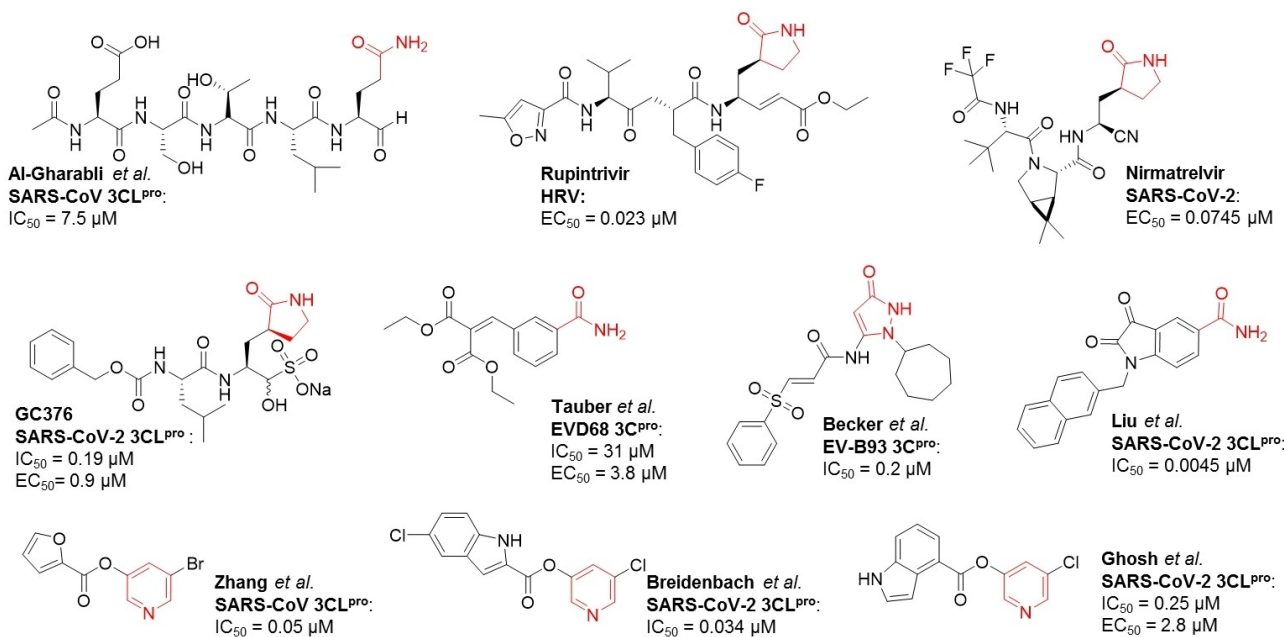


Figure 1. 3C and 3CL protease inhibitors reported in literature.^[6b,7d,8c,9a,10,12a,c,13,15a,b]

reactive electrophile such as a Michael acceptor, epoxide, vinyl sulfonamide, or an aromatic ketone for targeting the nucleophilic cysteine residue.^[6b,12] Several of these fragments displayed broad-band inhibition of 3C and 3CL proteases^[12a] and some were active in cellular virus proliferation assays, depending critically on the binding kinetics and chemical stability of the inhibitors.^[6b] All these reported fragments, however, failed as inhibitors of SARS M^{pro}. Instead, there have been several reports indicating that pyridine fragments might be the starting point for potent inhibitors of SARS-CoV-2 M^{pro}. Some 3-halopyridinyl esters were reported as potent inhibitors of SARS-CoV-1 main protease with IC₅₀ values as low as 50 nM^[13] and showed broad spectrum activity against other 3C proteases^[14] and recently of SARS-CoV-2 main protease.^[15] Although the reactivity of these active esters was suspected,^[16] a thorough investigation of the chemical and biochemical stability as well as of the kinetics of these molecules is missing so far. The same applies to thioesters being generally more reactive than the corresponding esters which were published as inhibitors of SARS-CoV-2 M^{pro} with reported activity in viral replication and infection assays, too.^[17] On the other hand, chemically stable pyridine fragments have found to bind to the S1 site of the SARS-CoV-2 main protease by using protein crystallography, however, with very low affinities.^[18] Moreover, studies on pyridine-containing peptidomimetics identified them as inhibitors of SARS-CoV-1 and SARS-CoV-2 M^{pro} with the pyridine residue binding to the S1 pocket of the protein, providing an essential interaction with the active site.^[19]

These studies raised the question, whether pyridine-containing fragments can be potent inhibitors of SARS-CoV-2 main protease with high activity, chemical stability, and sufficient target residence time. In this contribution we will answer this

question. For this purpose, a collection of pyridine-electrophile combinations was designed and synthesized to identify fragments which bind to the S1 pocket and react with the nucleophilic Cys-residue at the same time. In designing the library, we were especially interested in varying the distances between the pyridine fragment and the reactivity of the electrophiles, resulting in a set of compounds with a variation of the inhibition kinetics and, possibly, of their mode of action. We have also investigated the chemical stability of both inhibitors and of the protease-inhibitor complexes and will finally draw conclusions on the future potential and use of pyridine-containing SARS-CoV-2 main protease inhibitors.

Results and Discussion

Binding of the glutamine residue into the S1 pocket and interactions of the cleaved backbone amide with the catalytic site were analyzed using crystal structures of the peptide aldehyde Ac-ESTLQ-H with SARS-CoV-1 M^{pro} (PDB-ID: 3SND, Figure 2)^[7f] and the peptide cleavage product SAVLQ co-crystallized with the SARS-CoV-2 M^{pro} (PDB-ID: 7N6N, Supporting Information Figure 1)^[20] and suggested a binding mode of the intermediate of peptide bond cleavage shown in Figure 2a. In this the amide carbonyl of the glutamine residue interacted as an H-bond acceptor with the NH of the imidazole of His163 at the bottom of the S1 pocket and the amide-NH₂ as an H-bond donor to the backbone carbonyl groups of Phe140 and Glu166 (Figure 2a).^[6a] These interactions positioned the cleaved amide group in the catalytic center of the enzyme where the amide carbonyl is presumably activated by hydrogen bonds donated by backbone NH of Gly143 and Cys145 and attacked by the

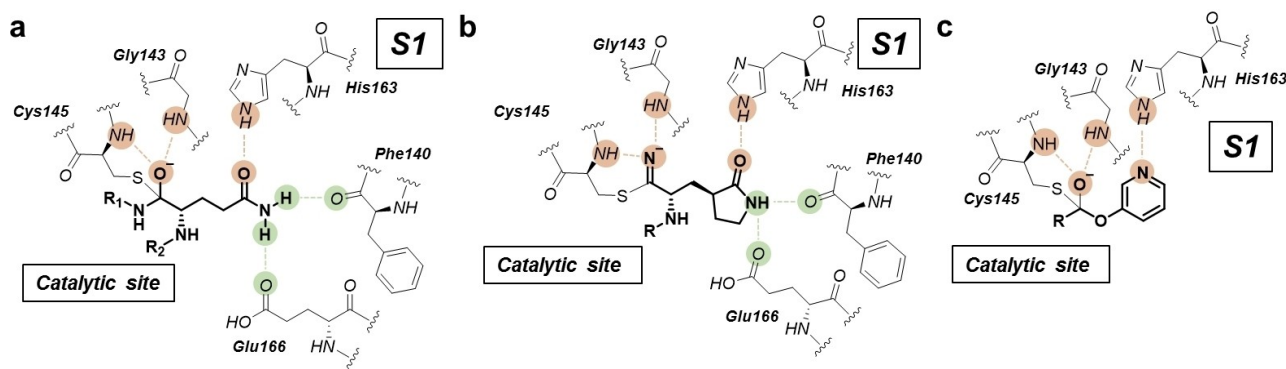


Figure 2. Postulated binding modes of a glutamine-containing peptide (a) as the natural substrate into the S1 pocket, the oxyanion hole and the covalent binding to the catalytic site Cys145 of the main protease of SARS CoV-2 and the comparison of the interactions with pyrrolidine-2-one derived from the crystal structure of nirmatrelvir (PDB-ID: 7VLP)^[21] (b) and pyridinyl esters (c).

nucleophilic thiolate residue of Cys145 yielding the tetrahedral intermediate. Similar interactions were found in peptidomimetics containing the pyrrolidin-2-one fragments instead of the glutamine residue, using the crystal structure of nirmatrelvir with the SARS-CoV-2 M^{Pro} (Figure 2b, PDB-ID: 7VLP).^[21] In conclusion, a potent covalent and reversible fragment inhibitor should provide hydrogen bonds with the S1 pocket, an electrophile for covalent interactions with the catalytic side, and a carbonyl oxygen or nitrile nitrogen for interactions with the oxyanion hole. In contrast, the covalent tetrahedral intermediate of pyridinyl-3-esters was not directly revealed from crystallization of the protein-ligand complex. Instead, as shown among others by Ghosh et al.^[15b] for a 5-chloropyridinyl-indole-2-carboxylate ester, the indole-2-carboxylate thioester with the thiol residue of Cys145 was formed (PDB-ID: 7RBZ). The proposed inhibition involved the catalytic dyad to form a tetrahedral intermediate, resulting in a covalent bound Cys145 of the SARS-CoV-2 M^{Pro}. According to the crystal structure of a small molecular ligand with a pyridine moiety (PDB-ID: 5R83) the S1 site provides similar interaction with the pyridine as the natural substrate glutamine (Supporting Information Figure 1).^[18] The pyridine ring nitrogen accepted a hydrogen bond of the imidazole ring of His163. Combination of these findings lead to the hypothesized binding mode shown in Figure 2c. Despite of these postulated interactions the high chemical reactivity and instability of pyridinyl esters raised the question, whether the strong inhibitory activity of **1** was the result of an unspecific acylation reaction or if they bind into the active pocket of the M^{Pro} of SARS-CoV-2 due to specific protein-ligand interactions.

Activity and stability of 5-bromo-pyridinyl-3-ester **1**

Inhibitor **1** with reported activity against the M^{Pro} of SARS-CoV-2^[13] (Figure 1) was resynthesized in our group and tested as an inhibitor of the main protease of SARS-CoV-2 in a fluorescence-based assay using the FRET substrate Dabcyl-KTSAVLQSGFRKME(Edans)-amide. When the inhibitor was incubated with the

enzyme for 30 s before adding the substrate, it revealed an IC₅₀ value of 15 nM (Table 1, for all methods and analytical data see Supporting Information). The high activity made this compound an interesting starting point for the development of acylating inhibitors. Next, the chemical stability of inhibitor **1** was investigated in the assay buffer (HEPES-EDTA, pH 8) without the target protease and DTT at room temperature (23 °C). After 30 min, degradation products were visible and after 24 h more than 90% of **1** was degraded according to HPLC-MS with UV detection at 254 nm (Figure 3a–c). Interestingly, compound **1** yielded three decomposition products, namely the furan-2-carboxylic acid **1a**, the 5-bromo-pyridin-3-ol **1b** and the transesterification product of **1** with HEPES, compound **1c**. As expected for a non-activated aliphatic ester, **1c** was stable toward hydrolysis under the assay conditions.

Derivatives of halopyridinyl esters with increased chemical stability

In order to improve the chemical stability of compound **1**, the pyridinyl ester moiety was replaced by more stable linkages and the obtained derivatives were tested in the protease assay. Replacement of the ester in lead compound **1** by an amide resulted in compound **2** (Table 1). Compound **2** showed 33% inhibition of the M^{Pro} at a concentration of 645 μM in the assay and, as expected, was completely stable under assay conditions. Replacement of pyridine by benzene yielded the 3-bromophenyl ester **3**, which displayed an IC₅₀ value of 14 μM, almost 1000 times higher than lead compound **1**. The considerably reduced activity of **3** could result from the missing interaction of the pyridine nitrogen with the amino acid His163 in the S1 pocket or from the lower reactivity of phenyl vs. pyridinyl ester with nucleophiles.

In order to increase the stability of pyridinyl esters while retain the pyridine fragment, a set of carbamates and carbonates was synthesized and the respective IC₅₀ values with SARS-CoV-2 M^{Pro} were determined (Table 1). The best inhibitor of this series was the 5-bromo-pyridinyl-ethyl carbonate **4**, being active

Table 1. Synthesized pyridinyl ester derivatives as inhibitors of the M^{pro} of SARS-CoV-2 and their inhibitory activity.^[a]

Compd	Inhibition at 645 μ M [%]	IC ₅₀ [μ M]
1 ^[b]	100	0.015
2	33	–
3	100	14
4	100	0.34
5	99	45
6	100	0.64
7	100	1.1
8	100	0.89
9	100	1.9
10	83	> 100
11	94	> 100
12	44	–
13	8	–
14	39	–
15	31	–
16	100	0.15 (0.034) ^[c]
17	100	0.19 (0.25) ^[c]

[a] Raw data and S.D. values are in the Supporting Information. [b] Compound 1 was already reported as an inhibitor of the M^{pro} of SARS-CoV-1 with an IC₅₀ of 50 nM.^[13] [c] Reported IC₅₀ values from literature.^[15a,b]

in the nanomolar range (0.34 μ M). The corresponding carbamate 5 was more than 100 times less potent with an IC₅₀ of 45 μ M. Compound 6, the 5-chloro analog of 4, showed a

small decrease of inhibitory activity with an IC₅₀ of 0.65 μ M. Increasing the size of the carbonate substituent from O-ethyl to O-benzyl, O-isobutyl, O-isopropyl or O-tert-butyl in compounds 7–10 consistently decreased the inhibitory potency. N-Phenyl carbamate 11 was only weakly active, while N-dimethyl carbamate 12, thiocarbamate 13 and the 5-bromo-pyridinyl-3-sulfonates 14 and 15 even at 645 μ M showed less than 50% inhibition. The 5-chloro-pyridinyl-3-esters 16^[15a] and 17^[15b,c, 22] were synthesized according to literature reports and showed similar inhibition of M^{pro} as the lead compound 1.

In general, all synthesized compounds showed higher IC₅₀ values compared to the original compound 1. Accordingly, we expected lower reactivity with nucleophiles and higher stability in buffer. Stability experiments with 4 over 24 h in HEPES-EDTA buffer at 23 °C showed improved stability with apparently less than 50% degradation after the experiment. (Figure 3d, e) Due to different UV absorption of compounds and degradation products a quantification of remaining inhibitor was difficult for both 1 and 4, respectively. For quantification of the degradation, representative compounds 1, 4–7, and 17, the latter reported to be active in VeroE6 cells infected with SARS-CoV-2,^[15b] were dissolved in HEPES-EDTA buffer at pH 8. Samples were taken at the beginning and every hour and measured with an LC/MS-QToF system for 15 h at 24 °C. The amount of remaining inhibitor was plotted against time in percent (Figure 3f). It was attempted to include compound 16 in this study, however, this reported inhibitor showed low solubility resulting in precipitation in buffer up to 10 μ M.

Bromo pyridinyl ester 1 was hydrolyzed rapidly to a remaining amount of about 20% after 15 h. Carbonates 4 and 6 displayed a higher resistance against nucleophiles and very similar stability with 62% and 63% remaining inhibitor, respectively. Apparently, the type of halogen atom (bromine vs. chlorine) had little impact on the stability. Carbamate 5 was less stable in assay buffer than the corresponding O-ethyl-carbonates 4 and 6 showing strong hydrolysis already after 1 h with a residual amount of only 18%. After 3 h, the compound was almost completely hydrolyzed, having a poorer stability than 1. This observation was interesting as carbamates have often been employed in drug design in order to increase the stability of esters.^[23] The observed chemical instability of 5 could be the reason for the lower inhibitory activity of this carbamate compared to the carbonates 4 and 6. Apparently in carbamate 5, n-electron donation by the N-ethyl substituent does not stabilize the carbamate through resonance, but instead accelerates elimination of the good leaving group 3-hydroxypyridine resulting in the intermediary formation of N-ethyl isocyanate. Subsequently, the isocyanate adds water and decarboxylates to the primary amine or can react further with another primary amine to deliver the N,N'-disubstituted urea as product. In the case of the N-phenyl carbamate 11, N,N'-diphenyl urea was indeed the main degradation product found already during synthesis and work-up. The higher reactivity of 11 can be explained by the favorable elimination of phenyl isocyanate. The proposed cleavage mechanism of carbamates can also rationalize the increased stability of compounds 12 and 13, which cannot eliminate isocyanate due to N,N-

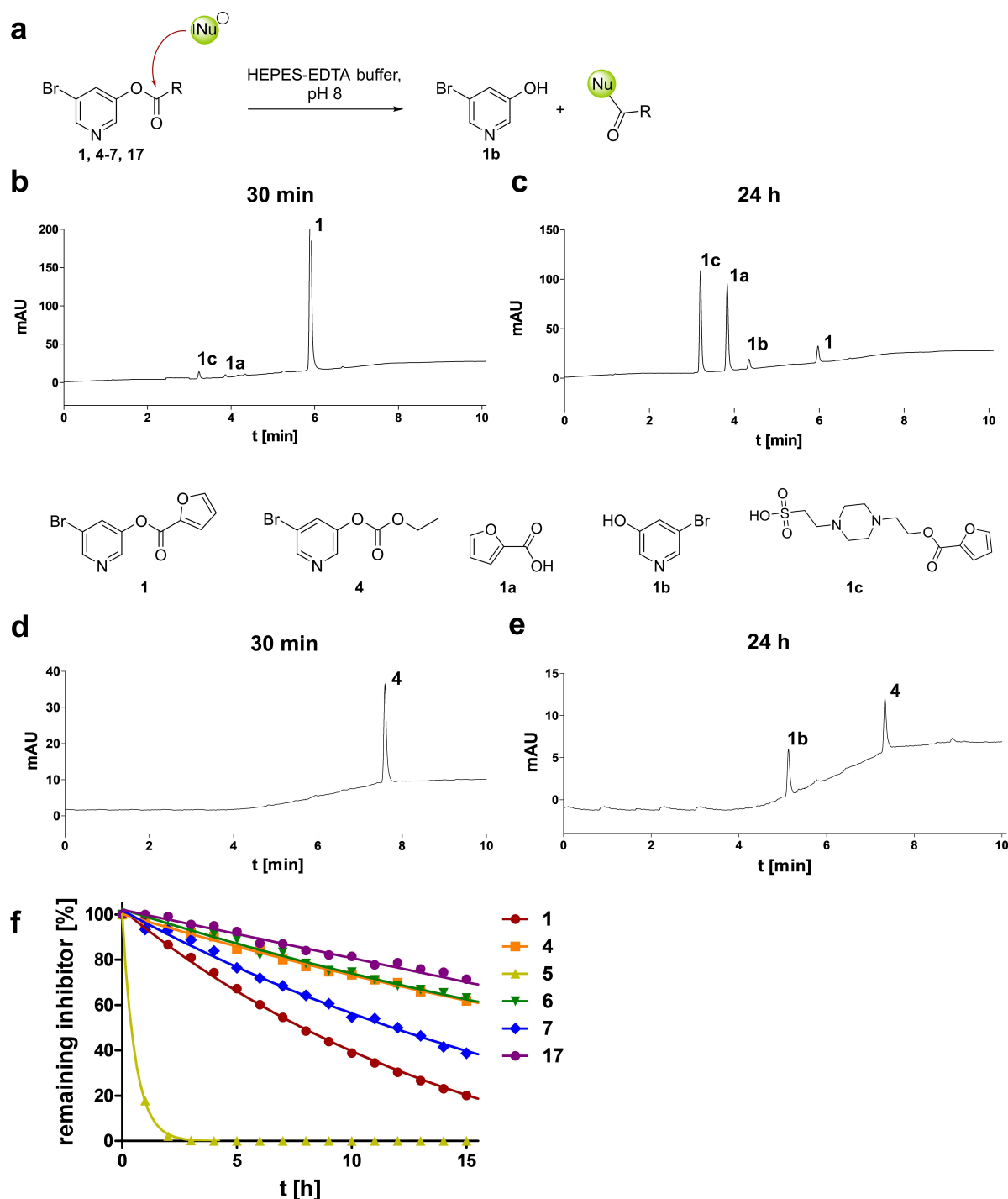


Figure 3. Chemical stability of protease inhibitors. **a.** Incubation of antiviral protease inhibitors in HEPES-EDTA buffer, pH 8 over time and their proposed mechanism of degradation. **b, c.** Incubation of 1 for 30 min and 24 h shows the instability toward nucleophiles, yielding hydrolysis products **1a** and **1b** as well as transesterification product **1c**. **d, e.** Incubation of compound 4 in HEPES-EDTA buffer indicates improved stability under FRET assay conditions. **f.** Quantitative determination of the degradation of compound 1, 4-7 and 17 in HEPES-EDTA buffer, pH 8 over 15 h at 24 °C.

disubstitution. The O-benzyl carbonate **7** showed higher stability than **1** with 39% residual compound at the end of the experiment but was less stable than the O-ethyl carbonates **4** and **6**. The ester **17** showed comparable stability as **4** and **6** with a residue of intact inhibitor of 71% after 15 h.

Characterization of reversibility and cellular testing

After evaluation of the chemical reactivity of our compounds, next thing was to characterize the stability of the covalent acyl-enzyme product. For this purpose, dilution assays were conducted with inhibitors **1**, **4**, **6**, **7**, **16**, and **17** to investigate

the kinetic stability of the covalent enzyme-inhibitor complex and the hydrolysis of the thioester bond to Cys145, respectively (Figure 4a). Inhibitors were tested in the FRET assay at 10-fold IC_{50} concentration showing the complete inhibition of SARS-CoV-2 M^{pro} under these conditions for all compounds but for inhibitor **1**, for which even at 10-fold IC_{50} concentration, the enzyme activity was restored gradually. In the dilution assay, the same inhibitors were first incubated with the enzyme at a 10-fold IC_{50} concentration. Subsequently, the samples were diluted by the factor of 100 to a concentration of $0.1 \times IC_{50}$ and measured in the FRET assay. In the case of reversible inhibitors, the protease activity will be restored after dilution, while irreversible inhibitors will show complete inhibition before and after dilution. For compounds **1** and **16**, the activity was completely and immediately restored, whereas **4**, **6**, **7** and **17** displayed the instantaneous but only partial recovery of the enzyme activity after dilution. These results suggest a reversible effect for all 6 compounds, but different stabilities of the acyl-enzyme intermediates. The carbonate inhibitors **4**, **6**, and **7** showed the lowest recovery of enzyme activity of less than 30% indicating the higher stability of protein thiocarbonate esters compared to protein thioester products derived from inhibitors **1** and **16**, and **17**.

In order to rationalize the binding modes of the most promising inhibitors **4** and **7**, we docked both compounds into the prepared X-ray crystal structure of M^{pro} (PDB-ID: 6Z2E)^[6a] as described in the Methods section. Both inhibitors establish the crucial hydrogen bond to the imidazole of His163 in the S1 pocket of the protease^[18] via the pyridine moiety. Both

inhibitors **4** and **7** establish lipophilic contacts between the pyridine moiety and bromide rest and side chains of the residues Phe140, Leu141, and Glu166 (Figure 5). The carbonyl group in both inhibitors shows two hydrogen bonds each to the NH group in the backbone of residues Gly143 and Cys145 placed in the oxyanion hole. These interactions might ensure a favorable geometry for the covalent binding to the closely placed sulfur atom of Cys145.^[18] The ethyl group in **4** and benzyl group in **7** establish lipophilic contacts to residues Thr25 and Leu27. The obtained favorable binding geometries for compounds **4** and **7** support the experimentally found building of stable covalent products.

As these improved stabilities of the inhibitors and their covalent enzyme products appeared to be very promising, investigation of the antiviral activity of **4** and **7** in infected Calu-3 cells with SARS-CoV-2 was performed. Both compounds were nontoxic toward human A549 cells up to 100 μ M (Figure 4b, SI). Unfortunately, the infection assay showed no inhibition of viral replication at 10 or 50 μ M with the compounds **4** and **7** (Figure 4c). One possible explanation could be still the lacking stability of the halopyridinyl carbonates.

Optimizing the pyridine- electrophile distance in SARS-CoV-2 M^{pro} inhibitors

Due to the rapid hydrolysis of pyridinyl esters and their protein acylation products, covalent reversible electrophiles were investigated in pyridine-electrophile combinations. In the first

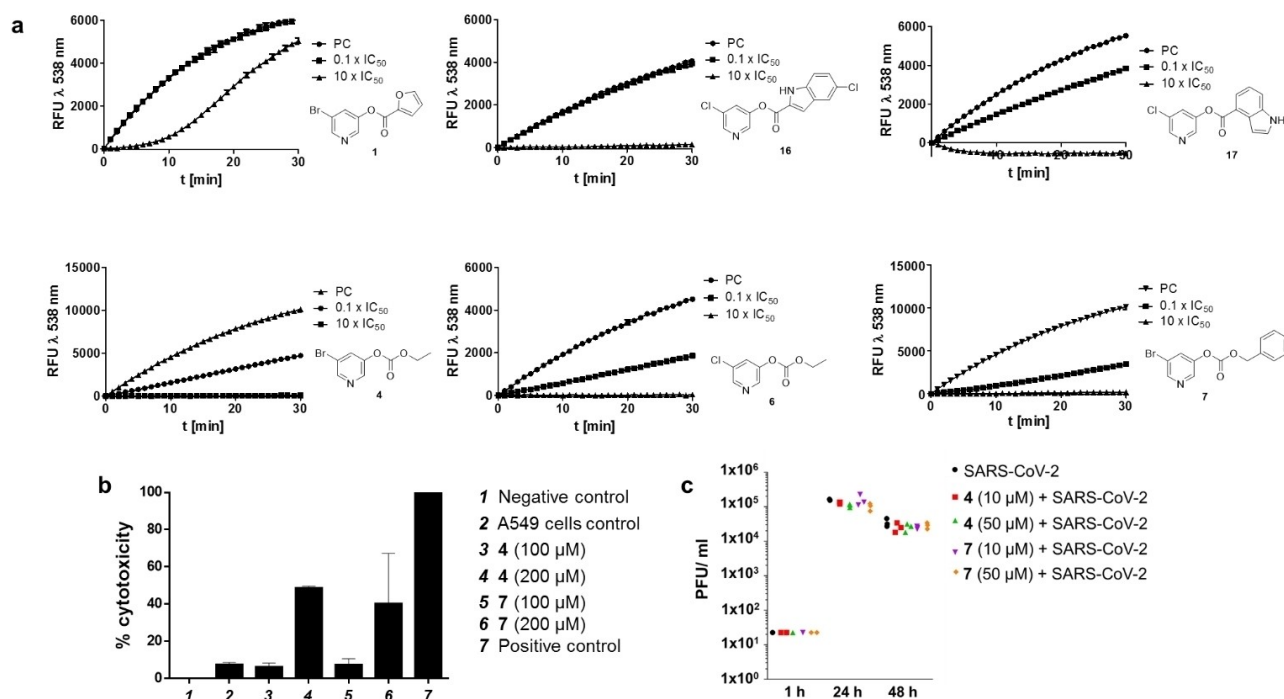


Figure 4. Stability of the enzyme-inhibitor complex and cellular testing. **a.** Dilution assays of **1**, **4**, **6**, **7**, **16** and **17** with the M^{pro} of SARS-CoV-2 from $10 \times IC_{50}$ to $0.1 \times IC_{50}$ revealed reversibility for all six inhibitors. Incomplete regeneration of protease activity with **4**, **6**, **7** and **17** might suggest higher stability of the acyl-enzyme products of these compounds. **b.** Compounds **4** and **7** displayed no cytotoxicity toward A549 cells up to 100 μ M. **c.** Infection assays of **4** and **7** with SARS-CoV-2 in Calu-3 cells showed no inhibition of viral replication at 10 and 50 μ M.

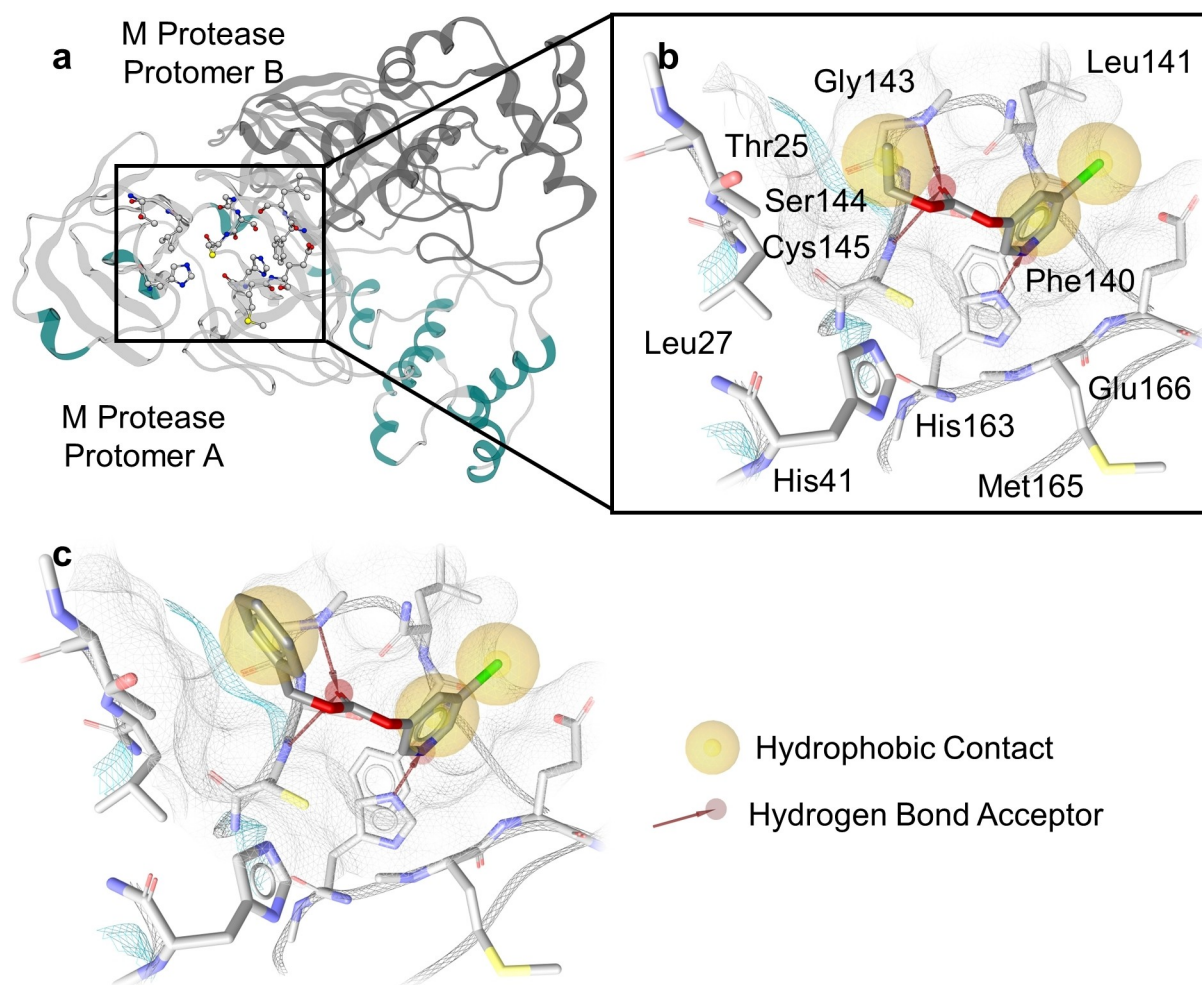


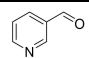
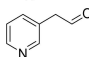
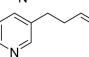
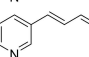
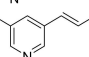
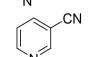
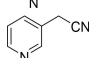
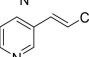
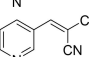
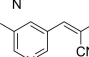
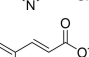
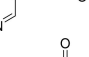
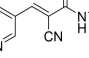
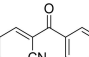
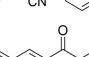
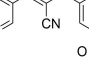
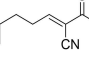
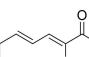
Figure 5. Binding hypotheses of inhibitors **4** and **7** in their noncovalent state before the addition-elimination reaction with the catalytic Cys145 of the M^{Pro} (grey and green ribbon). **a.** The global view on the M^{Pro} dimer and the substrate-binding site. Predicted binding modes of inhibitors **4** (**b.**) and **7** (**c.**). Color code: white spheres and grey sticks- carbon atoms, red spheres and sticks- oxygen atoms, blue spheres and sticks- nitrogen atoms, yellow sticks- sulfur atoms.

place, pyridine-aldehyde combinations **18–21** were obtained and tested in order to scrutinize various pyridine electrophile distances for inhibition (Table 2).

Nicotinaldehyde **18** showed partial inhibition of 27% at 1.6 mM concentration. The docking of **18** revealed that the carbonyl group of the inhibitor can reach the oxyanion hole and establish a covalent bond with Cys145 (Figure 6b). In additions, compound **18** displayed binding to the S1 pocket via the pyridine moiety and interacted with the imidazole residue of His163 as a hydrogen bond acceptor (Figure 6b). As a surrogate parameter for the strength of this hydrogen bond, we measured the angle between the nitrogen lone pair of the pyridine moiety in **18** and the imidazole N–H bond in His163 of ca. 140°. This value compared to a favorable range of 150°–180°^[24] suggested a weak hydrogen bond between **18** and His163 supporting the experimentally determined weak inhibitory activity. The homolog of **18**, 2-(pyridine-3-yl)-acetaldehyde **19** was predicted to bind to the imidazole of His163 via a hydrogen bond also with an H-bond angle of 140°, placing the carbonyl carbon of **19** closely to the thiol nucleophile of Cys145

and enabling H-bonding of the carbonyl oxygen with the side chain OH group of Ser144. Thus, the obtained docking pose suggested the subsequent formation of a covalent hemithioacetal intermediate (Figure 6c). Aldehyde **19** was prepared in 2 steps starting with a Grignard reaction of pyridine-3-yl magnesium bromide with allyl acetate yielding 3-allyl-pyridine **19a**.^[25] (see Supporting Information Figure 2) The allyl intermediate **19a** was bis-hydroxylated with ruthenium dioxide and cleaved in-situ using sodium periodate.^[26] Isolation of aldehyde **19** in pure form, however, was difficult due to the instability and high reactivity of this compound. Careful evaporation of solvents yielded compound **19** in monomeric form as indicated by LC–MS (see Supporting Information Figure 23). The crude product was tested directly after the synthesis for inhibitory activity against the M^{Pro} yielding 63% inhibition at 1.6 mM indicating an IC₅₀ value in the low mM range. Investigation of the stability revealed the clean oxidative degradation of **19** to the aldehyde **18** as proven by NMR. The further homologated 3-(pyridinyl-3)-propanal **20** was synthesized via an oxidation starting of the primary alcohol precursor and led to virtually

Table 2. Tested pyridinyl fragments with different electrophiles and their inhibitory activity against the M^{pro} of SARS-CoV-2.^[a]

Compd		Inhibition at 1.6 mM [%]	IC ₅₀ [μM]
18		27	–
19		62 ^[b]	–
20		95	117
21		100	25
22		100	1.8
23		13	–
24		20	–
25		50	–
26		89	81
27		87	22
28		33	–
29		83	> 400
30		93	117
31		96	94
32		71	> 500
33		96	155
34		84	80
35		99	86

[a] Raw data and S.D. are in the Supporting Information. [b] Tested from crude product.

complete inhibition of SARS-CoV-2 M^{pro} at 1.6 mM yielding an IC₅₀ value of 117 μM. The improved inhibitory activity of **20** compared to the compounds **18** and **19** correlated well with the docking experiment and suggesting that the electrophile in a meta-C3 position was superior to meta-C2 and meta-C1 positions. The obtained binding mode of **20** showed a hydrogen bond between the pyridine nitrogen of the inhibitor and the imidazole group of His163 in the S1 pocket (Figure 6d). The measured angular deviation of the N atom of pyridine moiety in **20** from the imidazole N–H plane in His163 of 170° was negligible indicating the formation of an energetically favorable

hydrogen bond. The oxygen atom of **20** establishes a hydrogen bond to the backbone amide NH group of Cys145 in the oxyanion hole, enabling the reversible formation of a covalent hemithioacetal intermediate (Figure 6d). The electrophilicity of the meta-C3 position was further increased by introducing an olefinic double bond in the side chain providing the more rigid 3-(pyridinyl-3)-prop-2-enal **21**. A Wittig reaction starting from nicotinaldehyde **18** furnished compound **21** with an E/Z ratio of 9:1, displaying a significantly improved IC₅₀ of 25 μM (Table 2). Introduction of the 5-bromo substituent in compound **22** further increased the inhibitory activity to an IC₅₀ value of 1.8 μM. The unsaturated aldehydes **21** and **22** were chemically stable other than the reactive aliphatic aldehyde **19**. According to modelling, compounds **21** and **22** docked into the S1 pocket enabling the attack of Cys145 at the olefinic C1 position, placing the aldehyde carbonyl into the oxyanion hole.

Next, we wanted to investigate, whether these activity-enhancing effects could be transferred to other C-electrophiles besides aldehydes. Nicotinonitrile **23** (with meta-C1 substitution) and 2-(pyridin-3-yl)-acetonitrile **24** (with meta-C2 substitution) showed only 13% and 20% inhibition at 1.6 mM, while homologation to meta-C3 substitution and desaturation to 3-(pyridin-3-yl)-acrylonitrile **25** increased inhibitory activity to 50%. As the nitrile residue was expectedly less electrophilic than an aldehyde residue, introduction of a second electron-withdrawing substituent was conducted to increase electrophilicity. As a result, 2-(pyridin-3-yl-methylene)-malononitrile **26** – the Knoevenagel product of **18** and malononitrile – was obtained improving the inhibitory potency strongly to an IC₅₀ value of 81 μM. Addition of another electron withdrawing group in compound **27**, the 5-bromo substituent, increased the inhibitory activity further to an IC₅₀ value of 22 μM. As seen before for the aldehydes **21** and **22**, the activities of nitriles **25**–**27** were increased by introduction of the electrophilic olefinic double bond enabling Michael addition of Cys145. Replacement of the nitrile substituent by the less electron-withdrawing and less electrophilic ethyl carboxylate in ethyl (E)-3-(pyridin-3-yl)-acrylate **28** displayed weaker inhibition with only 33% at 1.6 mM. The proposed mechanism of inhibition included the nucleophilic attack of the cysteine to the olefinic double bond instead of the ester carbonyl. However, additional modified analogues of this compound were not synthesized and investigated due to the poor inhibitory activity of **28**. Instead, further substituted acrylonitriles **29**–**35** were synthesized from pyridinyl-aldehydes **18**–**22** with CH acidic fragments using Knoevenagel condensation reactions, to create Michael acceptors with the same mechanism of inhibition as compound **28**. In all tested compounds the combination of the pyridine fragment with the acrylonitrile as electrophile led to inhibition of SARS-CoV-2 M^{pro}. Inhibitors **29**, **32**, and **33** with 2-cyano-acrylamides as electrophilic head group displayed 83%, 71%, and 96% inhibition at 1.6 mM, respectively. Stronger inhibition was observed for the cyano-ketones **30** and **34**. These structures were pyridine-3-yl-substituted 2-(4-methoxy-benzoyl)-acrylonitriles with IC₅₀ values of 117 and 80 μM, respectively. Introduction of 5-bromo substituent in both compounds led to **31** and **35** with IC₅₀ values of 94 μM and 86 μM (Table 2). Comparison

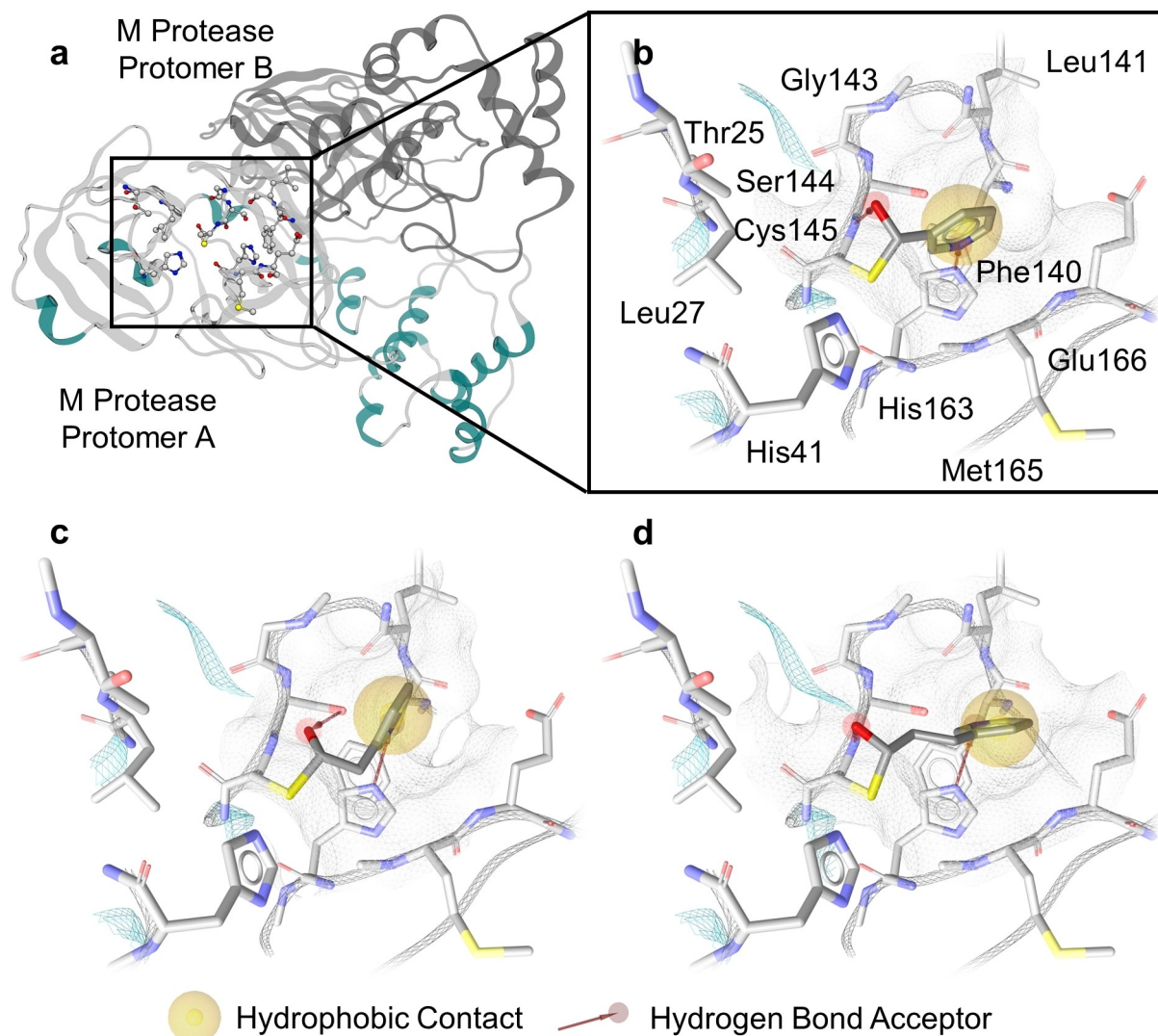


Figure 6. Binding hypotheses of inhibitors **18**, **19**, and **20** in their covalent state after the addition reaction with the catalytic Cys145 of the main protease (grey and green ribbon). **a.** The global view on the M^{pro} dimer and the substrate-binding site. Predicted binding modes of inhibitors **18** (**b.**), **19** (**c.**), and **20** (**d.**). Color code: white spheres and grey sticks- carbon atoms, red spheres and sticks- oxygen atoms, blue spheres and sticks- nitrogen atoms, yellow sticks- sulfur atoms.

of the IC_{50} values of all tested compounds reveal that aldehydes are superior to nitriles as electrophiles and electron withdrawing groups, which are more effective than keto- and amide substituents, preferably in meta-3C position to the pyridine fragment.

Conclusions

In this study we investigated the suitability of covalent, fragment-based inhibitors of the SARS-CoV-2 main protease containing the pyridine residue. In the first part, acylating inhibitors were investigated, including the 5-halo-pyridinyl-3-carboxylates **1**, **16**, and **17**, as well as the newly synthesized 5-halo-pyridinyl-carbonates **4** and **6–10** and the carbamate **5**. Several of these active esters and carbonates showed potent

inhibition of SARS-CoV-2 main protease in protein-based assays in the lower nanomolar range. A detailed investigation revealed that several of the inhibitors, especially active ester **1** and carbamate **5** hydrolyzed rapidly in physiological assay buffer, while carbonates **4**, **6** and **7** and the indole-carboxylate ester **17** were more stable. Even more relevantly, a kinetic dilution assay revealed that the acyl-enzyme intermediates formed during inhibition hydrolyzed rapidly under physiological assay conditions resulting in the irreversible deactivation of the inhibitors. Considering the numerous articles on acylating inhibitors of SARS CoV-2 main protease, we find this observation noteworthy. The new carbonates **4**, **6** and **7** displayed a higher stability against nucleophiles as well as a higher stability of the covalent protease-inhibitor complexes than the previously reported inhibitors **1**, **16**, and **17**. However, despite of their higher chemical and biochemical stability, the best pyridine-3-

carbonate esters **4**, **6** and **7** did not inhibit the proliferation of SARS-CoV-2 in virus-infected Calu-3 cells.

As a consequence, the development of covalent reversible pyridine-containing fragments with distinct binding affinity to the S1 pocket of the SARS-CoV-2 main protease was investigated as a starting point for chemically stable fragment-based inhibitors. A systematic variation of electrophiles with various distances to the pyridine fragment revealed the meta-3-position as being most effective for the simultaneous binding of the pyridine fragment to the S1 pocket of the enzyme, the nucleophilic attack of the Cys145 at the electrophile and the H-bonding of the latter to the oxyanion hole of the catalytic site. Aldehydes were found to be superior electrophiles to nitriles, ketones, and amide residues. The highest inhibitory activity was obtained for compound **22** with an IC₅₀ value of 1.8 μM, indicating high ligand efficiency of this small fragment with a molecular weight of 211 g/mol and constituting a powerful starting point for further drug development. These results confirm the possibility to develop covalent and reversible fragment inhibitors of SARS-CoV-2 main protease with pyridine binding to the active site, which might overcome the limitations of the acylating inhibitors reported before.

Experimental Section

Additional protocols and reaction schemes for the chemical synthesis of compounds **1–35** as well as other methodological information are reported in the Supporting Information. Identity and purity (>95%) of all compounds were determined by chromatography (silica or RP-18 HPLC), by fully assigned ¹H- and ¹³C-NMR spectra, by high-resolution mass spectra.

5-Bromopyridin-3-yl ethyl carbonate (4)

5-Bromopyridin-3-ol (201.6 mg, 1.16 mmol) was dissolved in DCM (4 ml). Diethyl dicarbonate (330 μl, 2.3 mmol) and scandium(III) trifluoromethanesulfonate (54.2 mg, 0.12 mmol) were added and the mixture was stirred at 40 °C for 23 h. After evaporation of the solvent, the residue was purified via MPLC (hexane/ ethyl acetate) yielding 5-bromopyridin-3-yl ethyl carbonate as a light yellow liquid (159.9 mg, 56%).^[27] ¹H NMR (600 MHz, DMSO-d₆): δ [ppm]=8.66 (d, J=2.0 Hz, 1H), 8.58 (d, J=2.1 Hz, 1H), 8.19 (t, J=2.2 Hz, 1H), 4.29 (q, J=7.1 Hz, 2H), 1.30 (t, J=7.1 Hz, 3H). ¹³C NMR (151 MHz, DMSO-d₆): δ [ppm]=152.28, 147.97, 147.58, 141.86, 132.33, 119.39, 65.40, 13.90. **ESI-HRMS**: [M+H⁺] calculated for C₈H₉BrNO₃⁺: 245.9760 Da, found: 245.9775 Da. **Rf**: 0.82 (hexane/ ethyl acetate, 50/50).

5-Bromopyridin-3-yl ethylcarbamate (5)

A Schlenk flask was heated and flushed with argon. 5-Bromopyridin-3-ol (200.1 mg, 1.15 mmol) was added and dissolved in dry DCM (4 ml). After cooling to 0 °C, triethylamine (30 μl, 0.23 mmol) and ethyl isocyanate were added dropwise via syringe. The mixture was stirred for 30 min at rt. After completion, the solvent was evaporated. The crude product was purified with MPLC (hexane/ ethyl acetate) and HPLC (water/acetonitrile with 0.1% TFA). Lyophilization in water/ acetonitrile yielded 5-bromopyridin-3-yl ethylcarbamate as a white solid (40.7 mg, 17%).^[28] ¹H NMR (500 MHz, DMSO-d₆): δ [ppm]=8.56 (dd, J=2.0, 0.4 Hz, 1H), 8.42 (dd, J=2.4, 0.5 Hz, 1H), 8.04–8.01 (m, 1H), 8.00 (t, J=2.2 Hz, 1H),

3.11 (m, J=7.2, 5.6 Hz, 2H), 1.09 (t, J=7.2 Hz, 3H). ¹³C NMR (126 MHz, DMSO-d₆): δ [ppm]=153.16, 147.94, 146.67, 142.19, 132.43, 119.25, 35.47, 14.68. **ESI-HRMS**: [M+H⁺] calculated for C₈H₁₀BrN₂O₂⁺: 244.9920 Da, found: 244.9927 Da. **Rf**: 0.29 (hexane/ ethyl acetate, 70/30).

Benzyl (5-bromopyridin-3-yl) carbonate (7)

A Schlenk flask was heated and flushed with argon. 5-Bromopyridin-3-ol (203.5 mg, 1.17 mmol) was dissolved in dry DCM (4 ml). The mixture was cooled to 0 °C and benzyl chloroformate (22 μl, 1.40 mmol) was added dropwise. After stirring for 2 h at rt, the reaction was diluted with DCM and washed with saturated sodium bicarbonate solution and water. Purification with MPLC (hexane/ ethyl acetate) of the crude product yielded benzyl (5-bromopyridin-3-yl) carbonate as a white yellow solid (270.9 mg, 75%).^[29] ¹H NMR (500 MHz, DMSO-d₆): δ [ppm]=8.67 (dd, J=2.0, 0.5 Hz, 1H), 8.60 (dd, J=2.3, 0.5 Hz, 1H), 8.23 (t, J=2.2 Hz, 1H), 7.51–7.35 (m, 5H), 5.31 (s, 2H). ¹³C NMR (126 MHz, DMSO-d₆): δ [ppm]=152.27, 148.07, 147.59, 141.83, 134.61, 132.31, 128.71, 128.60, 128.48, 119.41, 70.50. **ESI-HRMS**: [M+H⁺] calculated for C₁₃H₁₁BrNO₃⁺: 307.9917 Da, found: 307.9933 Da. **Rf**: 0.64 (hexane/ ethyl acetate, 70/30).

3-Allylpyridine (19a)

A Schlenk flask filled with Mg turnings (730.7 mg, 30 mmol), LiCl (1063.8 mg, 25 mmol) and a stirring bar was heated three times with a heat gun and flushed with argon after cooling down to room temperature. Dry THF (35 ml) was added followed by DIBAL-H (500 μl, 0.5 mmol). After 10 min of stirring at room temperature, 3-bromopyridine (1950 μl, 20 mmol) was added slowly to the mixture and stirred for 1 h. FeCl₃ (83.3 mg, 0.5 mmol) and allyl acetate (1101.3 mg, 10 mmol) were added and the mixture was stirred for another 15 min at room temperature before heating to 40 °C. The reaction was quenched after 30 min of heating with saturated sodium bicarbonate solution. The resulting mixture was extracted three times with ethyl acetate. The combined organic layers were washed with saturated sodium bicarbonate and dried with sodium sulfate. The brown liquid was purified with MPLC (DCM/ methanol). Careful removal of the solvent yielded 3-allylpyridine as a slightly yellow oil (472.5 mg, 36%).^[25] ¹H NMR (500 MHz, CDCl₃): δ [ppm]=8.46 (dt, J=3.1, 1.6 Hz, 2H), 7.50 (dq, J=7.8, 1.6, 0.9 Hz, 1H), 7.25–7.18 (m, 1H), 5.94 (ddtd, J=16.7, 10.1, 6.6, 1.4 Hz, 1H), 5.17–5.03 (m, 2H), 3.39 (dd, J=6.7, 1.6 Hz, 2H). ¹³C NMR (151 MHz, CDCl₃): δ [ppm]=150.22, 147.79, 136.29, 136.21, 135.40, 123.46, 116.92, 37.34. **ESI-MS**: [M+H⁺] calculated for C₈H₁₀N⁺: 120.08 Da, found: 120.0. **Rf**: 0.76 (DCM/ methanol, 90/10).

2-(Pyridin-3-yl)-acetaldehyde (19)

Sodium periodate (769.4 mg, 3.6 mmol) was dissolved in water (7 ml) and the pH was adjusted to 3–4 with 1 M HCl. 3-Allylpyridine (99.8 mg, 0.84 mmol), dissolved in DCM (7 ml) was added to the previous mixture. After cooling to 0 °C, ruthenium(IV) oxide (13.8 mg, 0.1 mmol) was added to the reaction and stirred for 2 h. The reaction was quenched with isopropanol (1 ml) and saturated sodium bicarbonate solution to adjust a pH of 8–9. The mixture was filtrated over Celite and extracted three times with DCM. The combined organic layers were washed with saturated sodium bicarbonate solution and dried over sodium sulfate. The solvent was evaporated carefully without heating and yielded 2-(pyridin-3-yl)-acetaldehyde **19** as yellow brown oil with impurities of aldehyde **18**. The crude product was tested immediately without further purification.^[26] As the compound was found to be very unstable, its

identity could only be confirmed by mass spectrometry. ESI-MS: [M + H⁺] calculated for C₇H₈NO⁺: 122.06 Da, found: 122.0 Da. Crude product **19** was quantitatively degraded oxidatively yielding a clean NMR spectrum of aldehyde **18** after 14 h.

3-(Pyridin-3-yl)-propanal (20)

In an oven dried Schlenk flask flushed with argon, DMP (769.0 mg, 1.81 mmol) was dissolved in dry DCM (4 ml) under argon atmosphere. After cooling to 0 °C, 3-(pyridin-3-yl) propan-1-ol (128.0 mg, 0.93 mmol) was added. The reaction was allowed to warm to room temperature and stirred for 4 h. The reaction was quenched with saturated sodium bicarbonate solution. The resulting mixture was extracted three times with ethyl acetate. After combining, the organic layers were washed with saturated sodium bicarbonate solution and dried with MgSO₄. Purification of the crude product with HPLC (water/ acetonitrile with 0.1% TFA) yielded 3-(pyridin-3-yl)-propanal as a yellow oil (44.8 mg, 36%).^[30] ¹H NMR (500 MHz, CDCl₃): δ [ppm] = 9.70 (d, J = 0.9 Hz, 1H), 8.87 – 8.64 (m, 2H), 8.25 (d, J = 8.0 Hz, 1H), 7.82 (s, 1H), 2.99 (dd, J = 7.8, 5.3 Hz, 2H), 2.95 – 2.90 (m, 2H). ¹³C NMR (151 MHz, CDCl₃): δ [ppm] = 202.21, 144.14, 142.80, 142.16, 43.22, 24.49. ESI-HRMS: [M + H⁺] calculated for C₈H₁₀NO⁺: 136.0757 Da, found: 136.0765 Da.

(E)/(Z)-3-(Pyridin-3-yl)-acrylaldehyde (21)

(Triphenylphosphoranylidene)-acetaldehyde (1339.7 mg, 4.4 mmol) was dissolved in dry toluene (27 ml) in an oven-dried Schlenk flask under argon atmosphere and 3-pyridinecarboxaldehyde (375 μl, 4 mmol) was added to the solution. The reaction was stirred for 24 h at 80 °C. After removal of the solvent, the residue was diluted with cold diethyl ether. The precipitate was filtered off and washed with cold diethyl ether. The filtrate was evaporated and purified with MPLC (hexane/ ethyl acetate) yielding (E)/(Z)-3-(pyridin-3-yl)-acrylaldehyde 9:1 as a yellow solid (393.8 mg, 74%).^[31] ¹H NMR (600 MHz, DMSO-d₆): δ [ppm] = 9.71 (d, J = 7.7 Hz, 1H), 9.62 (d, 0.1H), 8.91 (d, J = 2.3 Hz, 1H), 8.79 (d, 0.1 H), 8.64 (dd, J = 4.8, 1.6 Hz, 1H), 8.53 (dd, 0.1 H), 8.21 (dt, J = 7.9, 1.9 Hz, 1H), 8.06 (dt, 0.1 H), 7.79 (d, J = 16.1 Hz, 1H), 7.53 (d, 0.1H), 7.51– 7.48 (m, 1H), 7.45– 7.43 (m, 0.1H), 7.03– 6.99 (dd, J = 16.1, 7.7 Hz, 1H), 6.33– 6.29 (dd, 0.1H). ¹³C NMR (151 MHz, DMSO-d₆): δ [ppm] = 194.35, 194.20, 152.07, 151.63, 150.08, 150.00, 149.61, 149.15, 138.35, 135.07, 133.76, 132.20, 131.47, 130.10, 129.94, 128.66, 124.10, 123.97. ESI-HRMS: [M + H⁺] calculated for C₈H₇NO⁺: 133.0528 Da, found: 133.0521 Da. Rf: 0.25 (hexane/ ethyl acetate, 50/50).

(E)-3-(5-Bromopyridin-3-yl)-acrylaldehyde (22)

5-Bromopyridine-3-carbaldehyde (745.7 mg, 4.0 mmol) and (triphenylphosphoranylidene)-acetaldehyde (1340.3 mg, 4.4 mmol) were dissolved in an oven dried Schlenk flask under argon atmosphere in dry toluene (24 ml). The reaction was stirred for 24 h at 80 °C. After removal of the solvent, the residue was diluted with cold diethyl ether. The precipitate was filtered off and washed with cold diethyl ether. The filtrate was evaporated and purified with MPLC (DCM/ methanol) yielding (E)-3-(5-bromopyridin-3-yl)-acrylaldehyde as a beige solid (322.9 mg, 38%).^[31] ¹H NMR (600 MHz, DMSO-d₆): δ [ppm] = 9.70 (d, J = 7.6 Hz, 1H), 8.90 (d, J = 1.9 Hz, 1H), 8.76 (d, J = 2.2 Hz, 1H), 8.54 (t, J = 2.1 Hz, 1H), 7.74 (d, J = 16.1 Hz, 1H), 7.09 (dd, J = 16.1, 7.6 Hz, 1H). ¹³C NMR (151 MHz, DMSO-d₆): δ [ppm] = 194.28, 151.96, 148.48, 147.75, 137.29, 131.95, 131.38, 120.77. ESI-HRMS: [M + H⁺] calculated for C₈H₇BrNO⁺: 211.9706 Da, found: 211.9710 Da. Rf: 0.80 (DCM/ methanol, 90/10).

Stability testing of 1 and 4

For the stability testing of **1** and **4** inhibitor solution (10 μl, 20 mM in DMSO) were mixed with buffer (300 μl, 100 mM HEPES, 1 mM EDTA, pH 8) and shaken for 24 h at room temperature (22 °C). Samples were taken at 30 min and after 24 h and measured with an 1100 LCMS system with an UV detector at 254 nm. HPLC parameters: injection volume: 5 μl, column: Luna C18(2) (3 μm, 100 Å, 100 × 4.6 mm) from phenomenex, mobile phase: water (A), acetonitrile (B) with 0.1% formic acid, respectively, flow rate: 1 ml/min, gradient: 0–5.5 min from 95/5 (A/B) to 1/99 (A/B), 5.5–10 min 1/99 (A/B), 10–12 min from 1/99 (A/B) to 95/5 (A/B).

Quantitative monitoring of degradation

For the quantitative determination of the degradation of compound **1**, **4–7** and **17** inhibitor solutions (5 μl, 20 mM in DMSO) were mixed with buffer (995 μl, 100 mM HEPES, 1 mM EDTA, pH 8) and measured over time for 15 h at 24 °C with an Agilent 6550 iFunnel Qtof coupled with an Agilent 1290 Infinity II UHPLC. Samples were taken at the beginning and after every hour until the end of the experiment. The evaluation was performed with Masshunter QTOF-Quantification Software of Agilent. HPLC parameters: injection volume: 10 μl, column: Zorbax Eclipse plus C18 RRHD (1.8 μm, 95 Å, 2.1 × 50 mm) from Agilent, mobile phase: water (A), acetonitrile (B) with 0.1% formic acid, respectively, flow rate: 0.5 ml/min, gradient: 0–8 min from 95/5 (A/B) to 5/95 (A/B), 8–9 min 5/95 (A/B), 9–10 min from 5/95 (A/B) to 95/5 (A/B), 0–1 min and 6–10 min waste. Qtof parameters: positive mode, gas temperature 200 °C, gas flow 11 l/min, nebulizer 35 psig, sheath gas temperature 375 °C, sheath gas flow 11 l/min, octopole RF peak 750, fragmentor 175 V, nozzle voltage 500 V, Vcap 3500 V. Plotting of the percentage inhibitor concentration against the time and non-linear regression was performed with GraphPad Prism.

Dilution assays

All dilution assays were performed using the procedure adapted from Tauber et al.^[6b] A solution of SARS-CoV-2 M^{pro} (9 μl, 10 μM) was mixed with inhibitor stock solutions in DMSO (**1**: 1 μl, 2 μM, **4**: 35 μM, **6**: 65 μM, **7**: 100 μM, **16**: 15 μM, **17**: 20 μM). The inhibitor concentrations were chosen according to their IC₅₀ values resulting in total inhibition of the protease before dilution (10x IC₅₀). The mixture was shaken for 5 min and diluted afterwards with buffer (650 μl, 100 mM HEPES, 1 mM EDTA, 100 μM DTT, pH 8). To 20 μl of the diluted solution a FRET substrate solution (10 μl, 10 μM in buffer, 0.5% DMSO) was added and measured under FRET assay conditions. The resulting inhibitor concentration equated to 0.1 times the IC₅₀ value of the inhibitors. For controls SARS-CoV-2 M^{pro} (9 μl, 10 μM) was mixed with DMSO (**1**: 1 μl, 200 μM), **4** (1 μl, 3.5 mM), **6** (1 μl, 6.5 μM), **7** (1 μl, 10 mM), **16** (1 μl, 1.5 mM) or **17** (1 μl, 2 mM) and treated in the same way. The resulting inhibitor concentrations are 10 times higher than the IC₅₀ values.

Molecular docking

In order to rationalize the binding modes of the carbonate- (**4**, **7**) and aldehyde-containing inhibitors (**18**, **19**, **20**), the inhibitors were docked into the first-published X-ray crystal structure of the major protease (M^{pro}) from the severe acute respiratory syndrome coronavirus type 2 (SARS-CoV-2) with an atomistic resolution containing a substrate-mimetic inhibitor (PDB-ID: 6Z2E)^[6a] using GOLD (version 5.2; Genetic Optimisation for Ligand Docking, The Cambridge Crystallographic Data Centre, UK).^[32] The protein structure was prepared as a dimer that is the catalytically

competitive form.^[33] The water molecules, salt ions, and the co-crystallized ligand molecule were removed. The protein was protonated at pH of 7 and temperature of 300 K using Protonate3D^[34] algorithm included in MOE (version 2020.09, Molecular Operating Environment, Chemical Computing Group ULC, Montreal, Canada). The 3D conformations of compounds **4**, **7**, **18**, **19**, and **20** were prepared using Corina (version 3.0, Molecular Networks GmbH Computerchemie, Erlangen, Germany). Inhibitors **4** and **7** were docked into the prepared M^{pro} structure by performing ten genetic algorithm runs with 100% search efficiency. The ASP^[35] function was used for scoring and ChemScore^[36] for rescoring. The binding site was defined as a sphere with a radius of 12 Å around the sulfur atom in residue Cys145. The obtained docking conformations were minimized in the protein environment using the Merck molecular force field 94 s (MMFF94s)^[37] implemented in LigandScout4.3.^[38] The final binding hypothesis for each compound was selected based on the ability to establish crucial hydrogen bonds^[18] to i) the NH group in the imidazole ring of His163 in the S1 binding pocket and ii) the backbone NH group of Cys145 in the oxyanion hole as detected by LigandScout.

The inhibitors **18**, **19**, and **20** were covalently docked into the prepared M^{pro} structure using the same settings as for the inhibitors **4** and **7** described above. The sulfur atom in the catalytic residue Cys145^[18] in chain A was indicated as the covalently linking atom.

Author Contributions

R.W. and J.R. conceived and designed the experiments, R.W. and U.A. performed the experiments. R.W. and J.R. analyzed the data. M.B. and A.C.H. conducted viral infection experiments. S.P. and G.W. conducted computational studies. R.W. conducted chemical synthesis. C.A. conducted protein expression. R.W. and J.R. wrote the manuscript.

Acknowledgements

The authors acknowledge funding by the Deutsche Forschungsgemeinschaft (DFG, German Research Foundation) – Project-ID 387284271 – SFB 1349 (Project A3). U.B.A.A. received a graduate fellowship from the SFB 765. The work was supported by the DFG-funded core facility BioSupraMol and the Zentraleinrichtung für Datenverarbeitung (ZEDAT) of Freie Universität Berlin. A.C.H. was supported by DFG (SFB-TR 84), by BMBF (NUM-COVID 19, Organo-Strat 01KX2021), by BMBF (RAPID), and by Berlin University Alliance GC2 Global Health (Corona Virus Pre-Exploration Project). M.B. and A.C.H. were supported by Einstein Foundation EC3R. Open Access funding enabled and organized by Projekt DEAL.

Conflict of Interest

The authors declare no conflicts of interest.

Data Availability Statement

The data that support the findings of this study are available in the supplementary material of this article.

Keywords: Fragment-based drug discovery · SARS-CoV-2 main protease · antivirals · protease inhibitors

- [1] Z. Jin, X. Du, Y. Xu, Y. Deng, M. Liu, Y. Zhao, B. Zhang, X. Li, L. Zhang, C. Peng, Y. Duan, J. Yu, L. Wang, K. Yang, F. Liu, R. Jiang, X. Yang, T. You, X. Liu, X. Yang, F. Bai, H. Liu, X. Liu, L. W. Guddat, W. Xu, G. Xiao, C. Qin, Z. Shi, H. Jiang, Z. Rao, H. Yang, *Nature* **2020**, *582*, 289–293.
- [2] a) D. W. Kneller, G. Phillips, K. L. Weiss, S. Pant, Q. Zhang, H. M. O'Neill, L. Coates, A. Kovalevsky, *J. Biol. Chem.* **2020**, *295*, 17365–17373; b) F. Wu, S. Zhao, B. Yu, Y.-M. Chen, W. Wang, Z.-G. Song, Y. Hu, Z.-W. Tao, J.-H. Tian, Y.-Y. Pei, M.-L. Yuan, Y.-L. Zhang, F.-H. Dai, Y. Liu, Q.-M. Wang, J.-J. Zheng, L. Xu, E. C. Holmes, Y.-Z. Zhang, *Nature* **2020**, *579*, 265–269; c) P. Zhou, X.-L. Yang, X.-G. Wang, B. Hu, L. Zhang, W. Zhang, H.-R. Si, Y. Zhu, B. Li, C.-L. Huang, H.-D. Chen, J. Chen, Y. Luo, H. Guo, R.-D. Jiang, M.-Q. Liu, Y. Chen, X.-R. Shen, X. Wang, X.-S. Zheng, K. Zhao, Q.-J. Chen, F. Deng, L.-L. Liu, B. Yan, F.-X. Zhan, Y.-Y. Wang, G.-F. Xiao, Z.-L. Shi, *Nature* **2020**, *579*, 270–273.
- [3] C. A. Ramos-Guzmán, J. J. Ruiz-Pernía, I. Tuñón, *ACS Catal.* **2020**, *10*, 12544–12554.
- [4] a) M. J. Stoermer, *ChemRxiv. Cambridge: Cambridge Open Engage* **2020**; b) S. Ullrich, C. Nitsche, *Bioorg. Med. Chem. Lett.* **2020**, *30*, 127377.
- [5] a) C.-C. Lee, C.-J. Kuo, T.-P. Ko, M.-F. Hsu, Y.-C. Tsui, S.-C. Chang, S. Yang, S.-J. Chen, H.-C. Chen, M.-C. Hsu, S.-R. Shih, P.-H. Liang, A. H.-J. Wang, *J. Biol. Chem.* **2009**, *284*, 7646–7655; b) R. Ramajayam, K.-P. Tan, H.-G. Liu, P.-H. Liang, *Bioorg. Med. Chem.* **2010**, *18*, 7849–7854; c) R. Ramajayam, K.-P. Tan, P.-H. Liang, *Biochem. Soc. Trans.* **2011**, *39*, 1371–1375.
- [6] a) W. Rut, K. Groborz, L. Zhang, X. Sun, M. Zmudzinski, B. Pawlik, X. Wang, D. Jochmans, J. Neyts, W. Mlynarski, R. Hilgenfeld, M. Drag, *Nat. Chem. Biol.* **2021**, *17*, 222–228; b) C. Tauber, R. Wamsler, C. Arkona, M. Tügend, U. B. A. Aziz, S. Pach, R. Schulz, D. Jochmans, G. Wolber, J. Neyts, J. Rademann, *Angew. Chem. Int. Ed.* **2021**, *60*, 13294–13301; *Angew. Chem.* **2021**, *133*, 13405–13413.
- [7] a) P. S. Dragovich, S. E. Webber, R. E. Babine, S. A. Fuhrman, A. K. Patick, D. A. Matthews, S. H. Reich, J. T. Marakovits, T. J. Prins, R. Zhou, J. Tikhe, E. S. Littlefield, T. M. Bleckman, M. B. Wallace, T. L. Little, C. E. Ford, J. W. Meador, R. A. Ferre, E. L. Brown, S. L. Binford, D. M. DeLisle, S. T. Worland, *J. Med. Chem.* **1998**, *41*, 2819–2834; b) P. S. Dragovich, S. E. Webber, R. E. Babine, S. A. Fuhrman, A. K. Patick, D. A. Matthews, C. A. Lee, S. H. Reich, T. J. Prins, J. T. Marakovits, E. S. Littlefield, R. Zhou, J. Tikhe, C. E. Ford, M. B. Wallace, J. W. Meador, R. A. Ferre, E. L. Brown, S. L. Binford, J. E. V. Harr, D. M. DeLisle, S. T. Worland, *J. Med. Chem.* **1998**, *41*, 2806–2818; c) P. S. Dragovich, T. J. Prins, R. Zhou, S. A. Fuhrman, A. K. Patick, D. A. Matthews, C. E. Ford, J. W. Meador, R. A. Ferre, S. T. Worland, *J. Med. Chem.* **1999**, *42*, 1203–1212; d) S. I. Al-Gharabli, S. T. A. Shah, S. Weik, M. F. Schmidt, J. R. Mesters, D. Kuhn, G. Klebe, R. Hilgenfeld, J. Rademann, *ChemBioChem* **2006**, *7*, 1048–1055; e) M. F. Schmidt, A. Isidro-Llobet, M. Lisurek, A. El-Dahshan, J. Tan, R. Hilgenfeld, J. Rademann, *Angew. Chem. Int. Ed.* **2008**, *47*, 3275–3278; *Angew. Chem.* **2008**, *120*, 3319–3323; f) L. Zhu, S. George, M. F. Schmidt, S. I. Al-Gharabli, J. Rademann, R. Hilgenfeld, *Antiviral Res.* **2011**, *92*, 204–212.
- [8] a) P. S. Dragovich, T. J. Prins, R. Zhou, S. E. Webber, J. T. Marakovits, S. A. Fuhrman, A. K. Patick, D. A. Matthews, C. A. Lee, C. E. Ford, B. J. Burke, P. A. Rejto, T. F. Hendrickson, T. Tuntland, E. L. Brown, J. W. Meador, R. A. Ferre, J. E. V. Harr, M. B. Kosa, S. T. Worland, *J. Med. Chem.* **1999**, *42*, 1213–1224; b) P. S. Dragovich, T. J. Prins, R. Zhou, T. O. Johnson, Y. Hua, H. T. Luu, S. K. Sakata, E. L. Brown, F. C. Maldonado, T. Tuntland, C. A. Lee, S. A. Fuhrman, L. S. Zalman, A. K. Patick, D. A. Matthews, E. Y. Wu, M. Guo, B. C. Borer, N. K. Nayyar, T. Moran, L. Chen, P. A. Rejto, P. W. Rose, M. C. Guzman, E. Z. Dovalsantos, S. Lee, K. McGee, M. Mohajeri, A. Liese, J. Tao, M. B. Kosa, B. Liu, M. R. Batugo, J.-P. R. Gleeson, Z. P. Wu, J. Liu, J. W. Meador, R. A. Ferre, *J. Med. Chem.* **2003**, *46*, 4572–4585; c) F. G. Hayden, R. B. Turner, J. M. Gwaltney, K. Chi-Burris, M. Gersten, P. Hsyu, A. K. Patick, G. J. Smith III, L. S. Zalman, *Antimicrob. Agents Chemother.* **2003**, *47*, 3907–3916.
- [9] a) D. R. Owen, C. M. N. Allerton, A. S. Anderson, L. Aschenbrenner, M. Avery, S. Berritt, B. Boras, R. D. Cardin, A. Carlo, K. J. Coffman, A. Dantonio, L. Di, H. Eng, R. Ferre, K. S. Gajiwala, S. A. Gibson, S. E. Greasley, B. L. Hurst, E. P. Kadar, A. S. Kalgutkar, J. C. Lee, J. Lee, W. Liu, S. W. Mason, S. Noell, J. J. Novak, R. S. Obach, K. Ogilvie, N. C. Patel, M. Pettersson, D. K. Rai, M. R. Reese, M. F. Sammons, J. G. Sathish, R. S. P. Singh, C. M. Steppan, A. E. Stewart, J. B. Tuttle, L. Updyke, P. R. Verhoest, L. Wei, Q. Yang, Y. Zhu, *Science* **2021**, *374*, 1586–1593; b) J. Hammond, H. Leister-Tebbe, A. Gardner, P. Abreu, W. Bao, W. Wisemandle, M.

- Baniecki, V. M. Hendrick, B. Damle, A. Simón-Campos, R. Pypstra, J. M. Rusnak, *N. Engl. J. Med.* **2022**, *386*, 1397–1408.
- [10] a) C. Ma, M. D. Sacco, B. Hurst, J. A. Townsend, Y. Hu, T. Szeto, X. Zhang, B. Tarbet, M. T. Marty, Y. Chen, J. Wang, *Cell Res.* **2020**, *30*, 678–692; b) W. Vuong, M. B. Khan, C. Fischer, E. Arutyunova, T. Lamer, J. Shields, H. A. Saffran, R. T. McKay, M. J. van Belkum, M. A. Joyce, H. S. Young, D. L. Tyrrell, J. C. Vederas, M. J. Lemieux, *Nat. Commun.* **2020**, *11*, 4282.
- [11] I. F. Sevioukova, T. L. Poulos, *Proc. Natl. Acad. Sci. USA* **2010**, *107*, 18422–18427.
- [12] a) D. Becker, Z. Kaczmarek, C. Arkona, R. Schulz, C. Tauber, G. Wolber, R. Hilgenfeld, M. Coll, J. Rademann, *Nat. Commun.* **2016**, *7*, 12761; b) W. Liu, H.-M. Zhu, G.-J. Niu, E.-Z. Shi, J. Chen, B. Sun, W.-Q. Chen, H.-G. Zhou, C. Yang, *Bioorg. Med. Chem.* **2014**, *22*, 292–302; c) P. Liu, H. Liu, Q. Sun, H. Liang, C. Li, X. Deng, Y. Liu, L. Lai, *Eur. J. Med. Chem.* **2020**, *206*, 112702.
- [13] J. Zhang, H. I. Pettersson, C. Huitema, C. Niu, J. Yin, M. N. G. James, L. D. Eltis, J. C. Vederas, *J. Med. Chem.* **2007**, *50*, 1850–1864.
- [14] a) C. Huitema, J. Zhang, J. Yin, M. N. G. James, J. C. Vederas, L. D. Eltis, *Bioorg. Med. Chem.* **2008**, *16*, 5761–5777; b) I. Im, E. S. Lee, S. J. Choi, J.-Y. Lee, Y.-C. Kim, *Bioorg. Med. Chem. Lett.* **2009**, *19*, 3632–3636.
- [15] a) J. Breidenbach, C. Lemke, D. T. Pillaiyar, L. Schäkel, G. A. Hamwi, M. Dieltz, R. Gedschold, N. Geiger, V. Lopez, S. Mirza, D. V. Namasivayam, D. A. C. Schiedel, K. Sylvester, D. D. Thimm, C. Vielmuth, L. P. Vu, M. Zylina, P. D. J. Bodem, P. D. M. Gütschow, P. D. C. E. Müller, *Angew. Chem. Int. Ed.* **2021**, *60*, 10423–10429; *Angew. Chem.* **2021**, *133*, 10515–10521; b) A. K. Ghosh, J. Raghavaiah, D. Shahabi, M. Yadav, B. J. Anson, E. K. Lendy, S.-i. Hattori, N. Higashi-Kuwata, H. Mitsuya, A. D. Mesecar, *J. Med. Chem.* **2021**, *64*, 14702–14714; c) S. Hattori, N. Higashi-Kuwata, H. Hayashi, *Nat. Commun.* **2021**, *12*, 668.
- [16] a) J. Zhang, C. Huitema, C. Niu, J. Yin, M. N. G. James, L. D. Eltis, J. C. Vederas, *Bioorg. Chem.* **2008**, *36*, 229–240; b) H. Liu, S. Iketani, A. Zask, N. Khanizeman, E. Bednarova, F. Forouhar, B. Fowler, S. J. Hong, H. Mohri, M. S. Nair, Y. Huang, N. E. S. Tay, S. Lee, C. Karan, S. J. Resnick, C. Quinn, W. Li, H. Shion, X. Xia, J. D. Daniels, M. Bartolo-Cruz, M. Farina, P. Rajbhandari, C. Jurtschenko, M. A. Lauber, T. McDonald, M. E. Stokes, B. L. Hurst, T. Rovis, A. Chavez, D. D. Ho, B. R. Stockwell, *Nat. Commun.* **2022**, *13*, 1891.
- [17] T. Pillaiyar, P. Flury, N. Krüger, H. Su, L. Schäkel, E. Barbosa Da Silva, O. Eppler, T. Kronenberger, T. Nie, S. Luedtke, C. Rocha, K. Sylvester, M. R. I. Petry, J. H. McKerrow, A. Poso, S. Pöhlmann, M. Gütschow, A. J. O'Donoghue, Y. Xu, C. E. Müller, S. A. Laufer, *J. Med. Chem.* **2022**.
- [18] A. Douangamath, D. Fearon, P. Gehertz, *Nat. Commun.* **2020**, *11*, 5047.
- [19] a) M. D. Sacco, C. Ma, P. Lagarias, A. Gao, J. A. Townsend, X. Meng, P. Dube, X. Zhang, Y. Hu, N. Kitamura, B. Hurst, B. Tarbet, M. T. Marty, A. Kolocouris, Y. Xiang, Y. Chen, J. Wang, *Sci. Adv.* **2020**, *6*, eabe0751; b) C. Ma, Z. Xia, M. D. Sacco, Y. Hu, J. A. Townsend, X. Meng, J. Choza, H. Tan, J. Jang, M. V. Gongora, X. Zhang, F. Zhang, Y. Xiang, M. T. Marty, Y. Chen, J. Wang, *J. Am. Chem. Soc.* **2021**, *143*, 20697–20709; c) N. Kitamura, M. D. Sacco, C. Ma, Y. Hu, J. A. Townsend, X. Meng, F. Zhang, X. Zhang, M. Ba, T. Szeto, A. Kukuljac, M. T. Marty, D. Schultz, S. Cherry, Y. Xiang, Y. Chen, J. Wang, *J. Med. Chem.* **2022**, *65*, 2848–2865; d) J. K. Stille, J. Tjutris, G. Wang, F. A. Venegas, C. Hennecker, A. M. Rueda, I. Sharon, N. Blaine, C. E. Miron, S. Pinus, A. Labarre, J. Plescia, M. Burai Patrascu, X. Zhang, A. S. Wahba, D. Vlaho, M. J. Huot, T. M. Schmeing, A. K. Mittermaier, N. Moitessier, *Eur. J. Med. Chem.* **2022**, *229*, 114046; e) J. Jacobs, V. Grum-Tokars, Y. Zhou, M. Turlington, S. A. Saldanha, P. Chase, A. Egglar, E. S. Dawson, Y. M. Baez-Santos, S. Tomar, A. M. Mielech, S. C. Baker, C. W. Lindsley, P. Hodder, A. Mesecar, S. R. Stauffer, *J. Med. Chem.* **2013**, *56*, 534–546.
- [20] G. D. Noske, A. M. Nakamura, V. O. Gawriljuk, R. S. Fernandes, G. M. A. Lima, H. V. D. Rosa, H. D. Pereira, A. C. M. Zeri, A. F. Z. Nascimento, M. C. L. C. Freire, D. Fearon, A. Douangamath, F. von Delft, G. Oliva, A. S. Godoy, *J. Mol. Biol.* **2021**, *433*, 167118.
- [21] J. Li, C. Lin, X. Zhou, F. Zhong, P. Zeng, Y. Yang, Y. Zhang, B. Yu, X. Fan, P. J. McCormick, R. Fu, Y. Fu, H. Jiang, J. Zhang, *J. Virol.* **2022**, *96*, e02013–02021.
- [22] a) A. K. Ghosh, G. Gong, V. Grum-Tokars, D. C. Mulhearn, S. C. Baker, M. Coughlin, B. S. Prabhakar, K. Sleeman, M. E. Johnson, A. D. Mesecar, *Bioorg. Med. Chem. Lett.* **2008**, *18*, 5684–5688; b) S.-i. Hattori, N. Higashi-Kuwata, J. Raghavaiah, D. Das, H. Bulut, D. A. Davis, Y. Takamatsu, K. Matsuda, N. Takamune, N. Kishimoto, T. Okamura, S. Misumi, R. Yarchoan, K. Maeda, A. K. Ghosh, H. Mitsuya, L. M. Weiss, *mBio* **2020**, *11*, e01833–01820.
- [23] A. K. Ghosh, M. Brindisi, *J. Med. Chem.* **2015**, *58*, 2895–2940.
- [24] C. Bissantz, B. Kuhn, M. Stahl, *J. Med. Chem.* **2010**, *53*, 5061–5084.
- [25] M. Mayer, W. M. Czaplak, A. J. v. Wangelin, *Adv. Synth. Catal.* **2010**, *352*, 2147–2152.
- [26] K. H. Holm, D. G. Lee, L. Skattebøl, *Acta Chem. Scand.* **1978**, *32b*, 693–695.
- [27] G. Bartoli, M. Bosco, A. Carlone, M. Locatelli, E. Marcantoni, P. Melchiorre, P. Palazzi, L. Sambri, *Eur. J. Org. Chem.* **2006**, *2006*, 4429–4434.
- [28] R. C. Reynolds, A. Tiwari, J. E. Harwell, D. G. Gordon, B. D. Garrett, K. S. Gilbert, S. M. Schmid, W. R. Waud, R. F. Struck, *J. Med. Chem.* **2000**, *43*, 1484–1488.
- [29] J.-X. Xu, X.-F. Wu, *Org. Lett.* **2018**, *20*, 5938–5941.
- [30] M. Schönberger, D. Trauner, *Angew. Chem. Int. Ed.* **2014**, *53*, 3264–3267; *Angew. Chem.* **2014**, *126*, 3329–3332.
- [31] I. Hagedorn, W. Hohler, *Angew. Chem. Int. Ed.* **1975**, *14*, 486–486; *Angew. Chem.* **1975**, *87*, 486–486.
- [32] G. Jones, P. Willett, R. C. Glen, A. R. Leach, R. Taylor, *J. Mol. Biol.* **1997**, *267*, 727–748.
- [33] L. Silvestrini, N. Belhaj, L. Comez, Y. Gerelli, A. Lauria, V. Libera, P. Mariani, P. Marzullo, M. G. Ortoe, A. Palumbo Piccionello, C. Petrillo, L. Savini, A. Paciaroni, F. Spinuzzi, *Sci. Rep.* **2021**, *11*, 9283.
- [34] P. Labute, *Proteins* **2009**, *75*, 187–205.
- [35] W. T. M. Mooij, M. L. Verdonk, *Proteins* **2005**, *61*, 272–287.
- [36] C. A. Baxter, C. W. Murray, D. E. Clark, D. R. Westhead, M. D. Eldridge, *Proteins* **1998**, *33*, 367–382.
- [37] a) T. A. Halgren, *J. Comput. Chem.* **1996**, *17*, 490–519; b) T. A. Halgren, *J. Comput. Chem.* **1996**, *17*, 520–552; c) T. A. Halgren, *J. Comput. Chem.* **1996**, *17*, 553–586; d) T. A. Halgren, R. B. Nachbar, *J. Comput. Chem.* **1996**, *17*, 587–615; e) T. A. Halgren, *J. Comput. Chem.* **1996**, *17*, 616–641.
- [38] a) G. Wolber, T. Langer, *J. Chem. Inf. Model.* **2005**, *45*, 160–169; b) G. Wolber, A. A. Dornhofer, T. Langer, *J. Comput.-Aided Mol. Des.* **2006**, *20*, 773–788.

Manuscript received: November 23, 2022
Revised manuscript received: February 16, 2023
Accepted manuscript online: February 22, 2023
Version of record online: March 13, 2023